Gas barrier polymer nanocomposite films prepared by graphene oxide encapsulated polystyrene microparticles

Steven M.J. Merritt,[a] Alan M. Wemyss,[a] Stefano Farris,[b] Samson Patole,[c] Georgios Patias,[d] David M. Haddleton,[d] Barbara Shollock,[a] Chaoying Wan[a]*

a. International Institute for Nanocomposites Manufacturing (IINM), WMG, University of Warwick, CV4 7AL, UK

b. Department of Food, Environmental and Nutritional Sciences, University of Milan, Italy

c. TATA Steel Research and Development, Coventry, CV4 7EZ, UK

d. Department of Chemistry, University of Warwick, CV4 7AL, UK

ABSTRACT

The dispersion and orientation of two-dimensional (2D) inorganic nanoplatelets in polymers are technical challenges faced in polymer nanocomposite manufacturing. This work demonstrates an effective way to facilitate the dispersion and orientation of graphene oxide (GO) nanoplatelets in a polymer matrix through encapsulating the polymer within a nanoplatelet shell. Briefly, few-layered GO nanoplatelets encapsulated polystyrene (PS) microparticles were synthesized by a Pickering suspension polymerization method. The synthesis conditions, morphologies and barrier properties of the GO encapsulated PS spheres and the melt-compressed films are characterized.

The addition of salt induces flocculation of GO onto the surface of the styrene monomer droplet, resulting in the formation of a multi-layered GO shell as well as the sedimenting of the PS/GO particles during polymerization. The obtained GO encapsulated PS microspheres were purified, dried and melt-compressed to form composite films. The oxygen permeability (expressed as transmission rate) of the PS/GO composite film containing 2 wt% of GO was 526.02 ± 55.78 cm^3 m^{-2} 24 h^{-1}, a reduction of 96% relative to the PS control film, and 34% lower than the solution mixed PS/GO composite film. This indicates that the encapsulated PS spheres act as an effective carrier to facilitate the dispersion of GO. The orientation was realized by the following melt-compression process, which creates tortuous pathways hindering the permeation of gases through the PS matrix.

KEYWORDS: Encapsulation; Graphene oxide; Pickering suspension polymerization; Polymer nanocomposites; Gas barrier

INTRODUCTION

Polymeric materials are extensively used in the packaging industry, due to their low cost, ease of processing, diverse functionality and lightweight. However, most polymers are inherently permeable to small molecules due to their amorphous and semi-crystalline nature. The mechanical and barrier properties of a polymer can be enhanced by the inclusion of nanosized fillers.[1] The greatest improvement to barrier properties is observed in the application of two-dimensional (2D) nanoparticles in polymers, due to the formation of a tortuous permeation pathway, as a result of the large surface area and aspect ratio of the dispersed impermeable 2D nanoplatelets in the polymer matrices as dictated by the Nielson approximation.[2-3] The barrier properties of polymer nanocomposites are determined by the choice of nanofiller and the subsequent interfacial

interactions between nanofiller and matrix, as well as the extent of dispersion and orientation of the nanofiller within the matrix. Dispersion is affected by the compatibility between filler and matrix, with control over orientation achieved through strategies such as layer-by-layer assembly or application of a magnetic field to align particles. It is agreed that a well-exfoliated, ordered structure will possess enhanced barrier properties relative to aggregated and disordered structures.[4-8] The preparation of randomly orientated montmorillonite nanocomposite films, prepared by emulsion polymerization, has been reported to enhance oxygen barrier properties by only 30.3% at 1 wt% concentration, thus highlighting the need to develop methods that allow for simultaneous control over orientation and exfoliation.[9]

Control over the orientation of nanofiller has been achieved using emulsion polymerization by Heuts *et al.*, who demonstrated the encapsulation of both natural (montmorillonite)[10-11] and synthetic (gibbsite)[12-15] clays. Using atom transfer radical polymerization (ATRP) and reversible addition-fragmentation chain-transfer (RAFT) polymerization they prepared co-oligomers, which function as both the nanoparticle stabilizer and as a macro-initiator or macro-chain transfer agent for polymer chain extension.[12-16] Control over the particle morphology was reported *via* RAFT under starved fed conditions, where the clay sheets act as seeds for polymerization, forming anisotropic particles that align the nanoplatelets against the substrate in the cast film. Unfortunately barrier analysis was not conducted of these highly oriented materials.[16]

Graphene oxide (GO) is an ideal 2D nanoplatelet for barrier applications, in part due to its high aspect ratio (up to 10 μm) allowing for enhanced properties at lower filler loadings.[17-19] GO is widely used for modification of polymers due to its abundant oxygen-containing groups on the surface that benefit dispersion and interfacial interaction. Furthermore, the presence of hydroxyl, epoxy and carboxyl groups make GO amphiphilic, with the sp^2-bonded hexagonal carbon lattice

being the hydrophobic component, which makes it a viable candidate for use as a stabilizer for hydrophobic monomers in aqueous Pickering suspension polymerization.

A Pickering suspension polymerization is a heterogeneous polymerization system in which the monomer is stabilized by solid nanoparticles, omitting the need for molecular surfactants. Common Pickering stabilizers include laponite,[20-21] TiO_2,[22] and graphene oxide,[23-27] which have been demonstrated to stabilize hydrophobic polymers such as polystyrene (PS) and poly(methyl methacrylate). GO functions well as a stabilizer for the formation of emulsions due to its large surface area and amphiphilic nature, spontaneously self-assembling upon the oil surface and inhibiting coalescence.[23] Furthermore, with the desire to reduce the usage of volatile organic compounds (VOC), there is a demand for industrially viable waterborne methodologies.[5, 28]

In this study, we utilize GO encapsulated PS microparticles to control the dispersion and orientation of GO nanoplatelets in film coatings, which present efficient barrier properties. With a Pickering suspension polymerization method, the GO is utilized as the sole stabilizer for a styrene emulsion; sodium chloride (NaCl) is added to induce flocculation of the GO to the PS sphere surface. The addition of NaCl results in the polymerized GO encapsulated PS particles sedimenting from solution, allowing for facile isolation and salt removal. By this approach, we observe a significant improvement in oxygen barrier properties of the compressed PS/GO film, providing a 96% reduction with the addition of 2 wt% GO.

EXPERIMENTAL

Materials

Styrene (St, ≥99%; Sigma Aldrich) was purified by passing through a column of activated basic aluminium oxide (Sigma Aldrich). Azobisisobutyronitrile (AIBN, 98%, Sigma-Aldrich) and

sodium chloride (NaCl, Fisher Scientific) were used as received. Graphene oxide (GO, 97-98%; Abalonyx) was used as received. Deionized water was used in all experiments.

Synthesis

In a typical reaction, 1.0 wt% of GO aqueous dispersion was prepared by sonication for 1 hr using a Branson Digital Sonifier probe at 70% amplitude in an intermittent mode. The appropriate quantity of NaCl was subsequently added to the aqueous phase and stirred until fully dissolved. The organic phase, consisting of styrene (20 g, 0.175 mol) and AIBN (0.4 g, 2.44 mmol), was then mixed with the aqueous phase by magnetic stirring for 30 minutes followed by sonication with the sonifier probe at 70% amplitude for 30 minutes. The latter step was conducted in ice bath, with the probe used in short pulses, in order to avoid sample heating. The monomer emulsion was then deoxygenated for 40 minutes by nitrogen purging. Finally, the reaction was placed in an oil bath at 70 °C for 15 hours.

Following reaction completion, the PS/GO spheres were filtered and washed with deionised water to remove the NaCl. The solid was finally rinsed with methanol to obtain a free flowing powder. In all reactions, the concentration of NaCl was maintained constant relative to the GO content; with a targeted NaCl concentration of 300 mM for a 1 mg/mL GO dispersion. The concentrations used are given in Table 1. A polystyrene emulsion was also prepared using 2 wt% sodium dodecyl sulfate (SDS) and 1 mol% AIBN relative to the monomer as a control.

To compare the GO encapsulation PS microsphere composites with the equivalent composites voided of the armouring process, a PS/GO dispersion was prepared by solution mixing. GO was dispersed in THF with 1 hour sonication and resulted a 2 wt% dispersion. PS/SDS was dissolved in THF to make 10 wt% solution. The two solutions were mixed and stirred for 30 minutes then

cast into a glass petri dish. The samples were dried at 60ºC overnight, then compression moulded at 190°C for 5 minutes to obtain PS/GO composites with GO content of 1 and 2 wt%.

Table 1. NaCl/GO quantities for the preparation of the GO encapsulation PS. In all reactions styrene (20 g) and deionised water (400 mL) were used.

Sample Name	GO wt%	GO (mg)	NaCl (g)	NaCl concentration (mM)
PS/GO$_{0.2\%}$	0.2	40.1	0.7013	30
PS/GO$_{0.4\%}$	0.4	81	1.4026	60
PS/GO$_{0.5\%}$	0.5	99.1	1.7563	75
PS/GO$_{1\%}$	1	199.8	3.5054	150
PS/GO$_{2\%}$	2	399.6	7.0199	300
PS/GO$_{3\%}$	3	599.4	10.5162	450

CHARACTERIZATION

Size Exclusion Chromatography (SEC) data was collected using Agilent Infinity II MDS instrument equipped with differential refractive index (DRI), viscometry (VS), dual angle light scatter (LS) and multiple wavelength UV detectors, using a method described in the literature.[29] Briefly, chloroform containing 2% TEA (triethylamine) was used as eluent, polystyrene standards (Agilent EasyVials) were used for calibration, and ethanol was added as a flow rate marker. The samples were filtered through a GVHP membrane with 0.22 μm pore size before injection. The samples were run at 1 mL/min at 30°C, experimental molar mass (M_n,SEC) and dispersity ($Đ$) values of the synthesized polymers were determined by using Agilent GPC/SEC software. Fourier-transform infrared (FT-IR) spectra were recorded on a Bruker Spectrometer with a scan range from to 4000 cm^{-1} to 500 cm^{-1}.

Particle size and morphology were studied by scanning electron microscopy (SEM, Carl Zeiss Sigma Field SEM) and transmission electron microscopy (TEM, Jeol 2100, fitted with a Gatan Ultrascan 1000 camera). For SEM, the particle samples were deposited onto a fresh silica sheet, then subsequently air-dried and gold sputter coated. Film samples were cryo-fractured then gold sputter coated. Samples were analyzed at accelerating voltages between 5 and 10 kV. The emulsion sample was diluted at 0.1 vol% and casted on a carbon coated copper grid for TEM analysis.

Cross-section images of PS/SDS and nanocomposite films were acquired using an optical microscope (Micro Nikon Eclipse ME600 Laboratory Imaging, Nikon Instruments, Sesto Fiorentino, Italy). Films after storage (2 weeks in a desiccator) were cut with a sharp razor blade. The thickness of the films was recorded at a 20× magnification, whereas information on the filler distribution was obtained at 100× magnification. The software NIS-Elements BR 5.11.00 (Nikon Instruments, Sesto Fiorentino, Italy) was used for data analysis.

Thermogravimetric Analysis (TGA) was carried out using a Mettler Toledo thermal analyser over the temperature range of 25°C to 1000°C at a heating rate of 10°C min^{-1} under nitrogen.

The oxygen barrier properties of the PS/SDS and PS/GO films (obtained by compression-moulding of GO encapsulation PS spheres and PS/GO solution-mixed samples) were assessed using a Multiperm Permeability Analyser (Extrasolution Srl, Capannori, Italy) equipped with an electrochemical sensor. Specimens were sandwiched between two aluminum-tape masks, allowing a surface of 2.5 cm^2 to be exposed to the permeation of oxygen. The oxygen transmission rate (OTR, $cm^3\ m^{-2}\ 24\ h^{-1}$) was determined according to the standard method of ASTM F1927,[30] with a carrier N_2 flow of 70 mL min^{-1}at 23°C and 80% relative humidity (RH). Each OTR value was averaged from three replicates.

RESULTS AND DISCUSSION

Particle characterisation

PS was synthesized using emulsion polymerization, with AIBN as the initiator and SDS as the surfactant. The resulting latex has a particle size of ~250 nm, as shown by SEM (Figure S2). When compared with solution or bulk polymerization with equivalent monomer and initiator concentrations, emulsion polymerization results in higher molecular weights due to the segregation of the propagating radicals in the system, which lowers the rate of bimolecular termination, allowing chains to grow longer. SEC analysis of the dried PS particles, given in Figure 1, showed that a molecular weight (M_n) of 97,000 g/mol was achieved.

GO encapsulated PS microparticles were prepared by Pickering suspension polymerization, with 300 mM of NaCl added to the continuous phase per 1 mg/mL of GO. The GO/monomer suspensions were found to be adequately stable. During polymerization, the particles sediment from the suspension, leaving a clear aqueous phase. The particle sedimentation allowed for exceptionally facile work up *via* decanting followed by washing of the product with ~2 L DI H_2O to ensure full removal of NaCl.

The introduction of NaCl prior to preparation of the monomer suspension results in charge screening of the oxygen containing hydroxyl and carboxylic acid groups in GO.[23, 31] As the concentration of NaCl increases the negative zeta potential of the system tends towards zero, reducing the intersheet electrostatic repulsion and inducing flocculation and stacking of the GO sheets.[23, 32-33] In our experiment, the probe sonication used to disperse the GO sheets reduced their diameter slightly, as shown in Figure S6, however they are still present as multilayer stacks approximately 10 μm in diameter. These larger particles form larger droplets in a Pickering

stabilized system, and the stability of the monomer suspensions is worth investigating. Figure S1A shows optical microscopy images of a PS/$GO_{3\%}$ suspension prior to polymerization. The droplet size was found to be 8~10 μm and with constant stirring the suspensions were found to be relatively stable for at least 4 days (Figure S1B). The PS/$GO_{0.2\%}$ suspension displayed colloidal instability, most likely due to their being insufficient GO present to stabilize the styrene.

To assess the molecular weight distributions of the PS formed in our Pickering system, it was extracted from the GO encapsulated microparticles with chloroform and analyzed by SEC. Their molecular weights and polydispersity indices ($Đ$) are given in Table 2 and Figure 1.

Table 2. Obtained number average molecular weight (M_n) and weight average molecular weight (M_w) of polystyrene for each sample with calculated dispersity ($Đ$)

Sample	M_n (g/mol)	M_w (g/mol)	$Đ$
PS/SDS	97,000	290,000	3.00
PS/GO$_{0.4\%}$	42,000	209,000	4.92
PS/GO$_{0.5\%}$	36,000	179,000	5.01
PS/GO$_{1\%}$	42,000	195,000	4.69
PS/GO$_{2\%}$	42,000	188,000	4.51
PS/GO$_{3\%}$	43,000	212,000	4.94

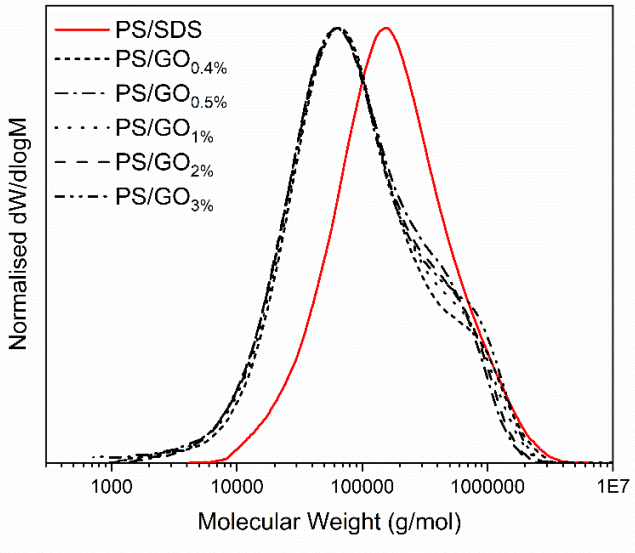

Figure 1. SEC traces of PS isolated from GO microparticles using chloroform as the eluent.

As shown in Figure 1, it is apparent that all PS/GO samples display a similar peak molecular weight, irrespective of the GO content, and each have a high molecular weight shoulder that corresponds approximately to the PS/SDS peak molecular weight. These bimodal peaks indicate the presence of two discrete species of polymer present in the PS/GO samples. The lower molecular weight PS is likely formed within the core of the large particles, where the conditions

are similar to a bulk polymerization process, resulting in a relatively low molecular weight product. Whereas, the presence of the high molecular weight shoulder peaks indicates that a lesser quantity of smaller PS particles are present, which are better segregated and polymerize like in emulsion polymerization. Small beads of approximately ~250 nm in diameter were observed in the outer shell of the PS/GO spheres (Figure 2A-D), which is similar to the size observed in PS/SDS emulsions (Figure S2).

ImageJ software was used to determine the average particle size of the PS/GO samples from their SEM images, with at least 20 particles recorded per image. The results shown in Table 3 indicate a reasonably consistent particle size for each of the sample preparations. Repeated preparations at the same GO concentration also produced consistent results, as shown in Figure S3, where good agreement between the SEC traces of two separate $PS/GO_{1\%}$ samples was obtained, and similar particle size and surface texturing was observed under SEM.

Table 3 Particle sizes determined by SEM and ImageJ.

Sample	Particle size (μm)	Standard Deviation (σ)
PS/GO$_{0.4\%}$	4.00	0.84
PS/GO$_{0.5\%}$	4.14	1.09
PS/GO$_{1\%}$	3.60	0.98
PS/GO$_{2\%}$	3.80	1.19
PS/GO$_{3\%}$	5.00	0.91

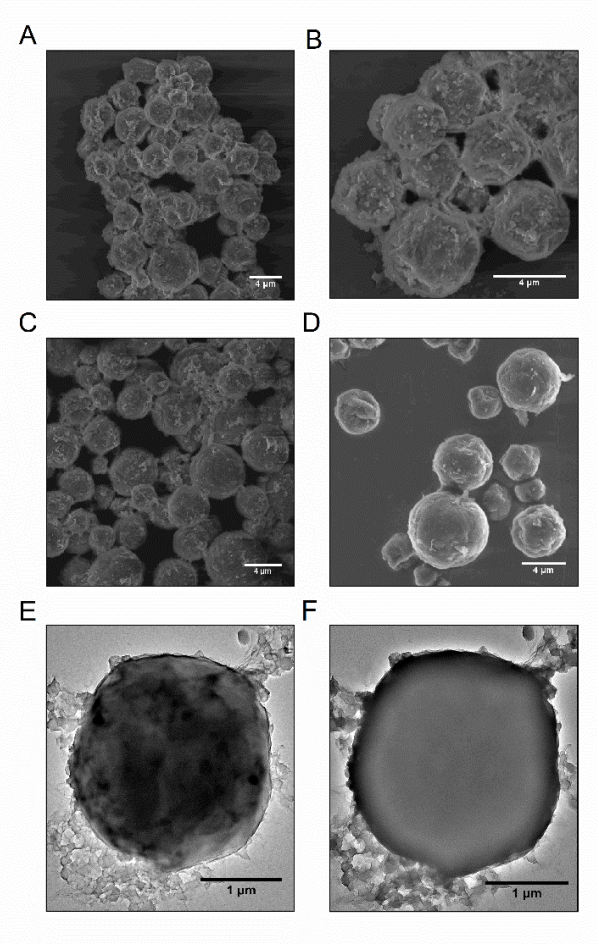

Figure 2. SEM secondary electron images of processed GO encapsulated particles. A) PS/GO$_{0.4\%}$. B) PS/GO$_{0.5\%}$. C) PS/GO$_{1\%}$. D) PS/GO$_{2\%}$. E) TEM image focused upon surface of

PS/$GO_{1\%}$. F) TEM image focused on the interior of the GO shell of PS/$GO_{1\%}$. Scale Bars: A-D = 4 μm, E-F = 1 μm.

Interestingly, whilst increasing the GO content appears to have little impact upon particle size or molecular weight of the polystyrene, the surface texturing of the particles is significantly different between those with 0.4 wt% and 2 wt% loading of GO (Figure 2). It is apparent that as the GO loading increases the GO shell thickness increases, masking the previously observed texturing at lower GO loadings, to obtain smoother particles. As discussed above, all samples display evidence suggesting the presence of small, higher molecular weight PS beads located within the shell of the particle, and also visualized in Figure 2A-D. The TEM image in Figure 2E shows the surface texture of a PS/$GO_{1\%}$ particle, and if the focal plane is dropped down into the PS/GO particle, a homogenous PS core is observed, as shown in Figure 2F.

Film characterisation

The PS/SDS and PS/GO spheres were compression-moulded to form thin films at 190^{o}C, the film thickness is 110 ~130 μm as determined by optical microscopy (Figure S5). The cross-section of the PS/SDS film, Figure 3A, displays a smooth surface. The PS/GO composite film displays texturing in Figure 3B-C, and the oval contour indicates the compressed PS/GO spheres according to the dimension of the particles, which displays a clear GO shell aligned perpendicular to the permeation pathway, induced by the compression moulding. Interestingly, traces of the particle may be observed in the cross section in the form of dark circular rings, shown in Figure 3D. These structures are not observed in the PS/SDS control images, given in Figure 3A**,** and are concluded to be part of the GO shell from the PS/GO particles.

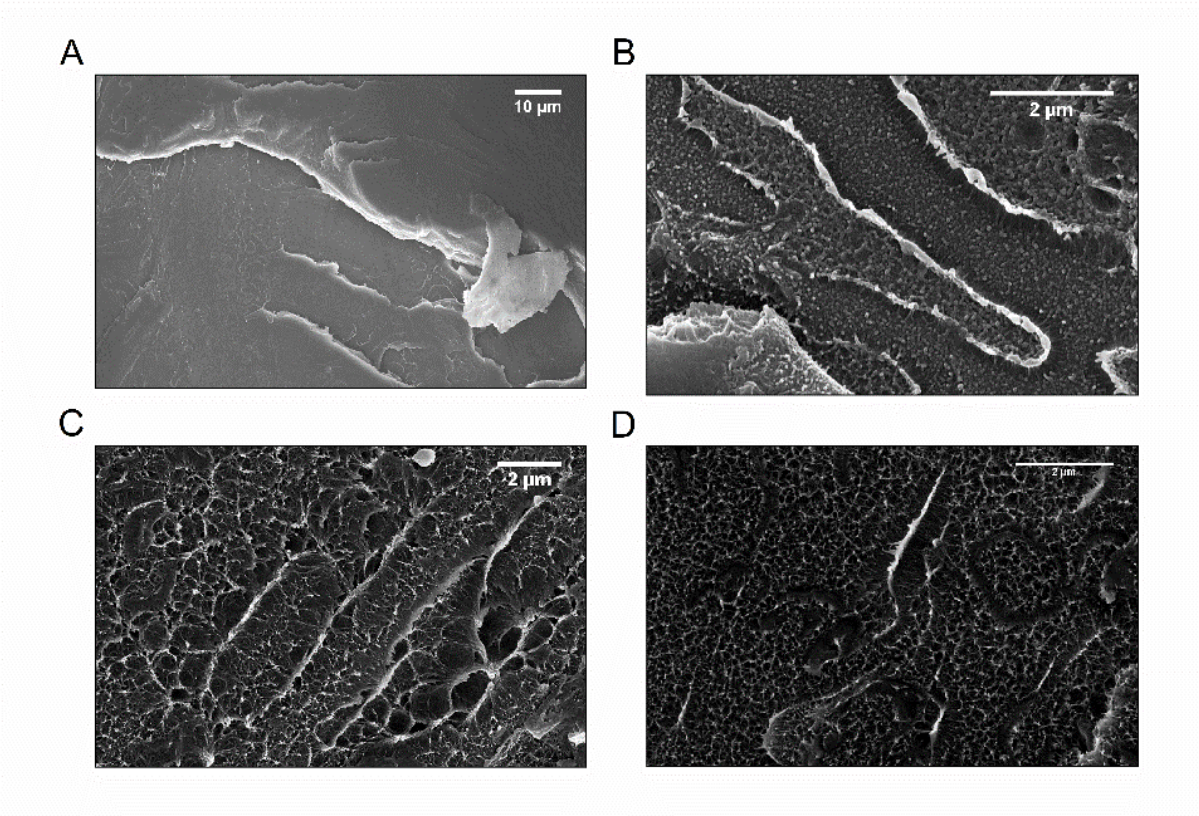

Figure 3. SEM secondary electron cross sections of A) PS/SDS film; and B, C) and D) different sections of PS/$GO_{1\%}$.

The PS/GO spheres were also compressed at 120°C alongside 190°C to evaluate the effect of compression temperature upon the film forming as well as the degree of GO reduction. As shown by Raman (Figure S7) and IR spectroscopy (Figure S8), the higher temperature compression moulding did not cause detectable reduction of the GO. However, the lower temperature compression moulding resulted in films that contained trace quantities of non-melted particles embedded within the film (Figure S9). As such, the composite films compressed at higher temperature (190°C) were used for oxygen barrier characterization.

Three representative OTR plots for the pristine PS/SDS films and PS/GO films with 1 wt% and 2 wt% GO are given in Figure 4. The OTR values for the PS/SDS film (14464.67 ± 1050.43 cm^3

m^{-2} 24 h^{-1}, thickness 120.4 ± 9.3 μm) are in line with data reported in the literature,[34-35] which denotes PS as a poor oxygen barrier material. The addition of 1 wt% GO decreased the OTR to 1019.15 ± 97.35 cm^3 m^{-2} 24 h^{-1} (thickness 130.5 ± 11.2 μm), which is comparable with the oxygen barrier performance of a 30 μm bi-oriented polypropylene film (OTR ~ 866 mL·m^{-2}·24 h^{-1}).[36] The nanocomposite film with 2 wt% of GO experienced an additional ~96% reduction, with a final OTR value of 526.02 ± 55.78 cm^3 m^{-2} 24 h^{-1} (thickness 110.1 ± 9.8 μm), comparable with a 25 μm polylactic acid film (746 cm^3 m^{-2} 24 h^{-1}).[37]

In our previous work, pullulan/GO nanocomposite films were prepared using a direct solution-mixing method.[38] It is shown that with a loading of 0.3 wt% of GO, the OTR of the pristine pullulan film was reduced from 181.04 ± 20.05 cm^3 m^{-2} 24 h^{-1} (i.e., $P'O_2$ ~ 6337 mL μm m^{-2} 24 h^{-1}) to 33.09 ± 2.94 cm^3 m^{-2} 24 h^{-1} (i.e., $P'O_2$ ~ 1357 mL μm m^{-2} 24 h^{-1}, thickness ~ 40 μm) measured at 23°C and 70% RH. When the pullulan/GO nanocomposite was coated onto a polyethylene terephthalate film (PET, 12 μm thick),[39] the OTR of the coated PET was dropped below the detection limit of the instrument (< 0.01 mL μm m^{-2} 24 h^{-1}) even when the GO concentration was as low as 0.04 wt%. However, a dramatic increase of the OTR values occurred in humid conditions, at 90% RH, the OTR of the coated PET films was ~ 100 mL m^{-2} 24 h^{-1}, similar to that of bare PET films. Recently, a spray-assisted layer-by-layer assembly method was used to couple GO (negatively charged) and amino-functionalized GO (positively charged).[40] The alternating layers of GO (-) and amino-GO (+) were deposited on polyethylene (PE, 50 μm thick) which has no intrinsic gas barrier properties (OTR ~ 3500 mL m^{-2} day^{-1}, i.e., $P'O_2$ ~ 175000 mL μm m^{-2} 24 h^{-1}). The layer of GO coating with thickness of just 60 nm significantly reduced the OTR to 1091 mL m^{-2} day^{-1} (i.e., $P'O_2$ ~ 54600 mL μm m^{-2} day^{-1}).

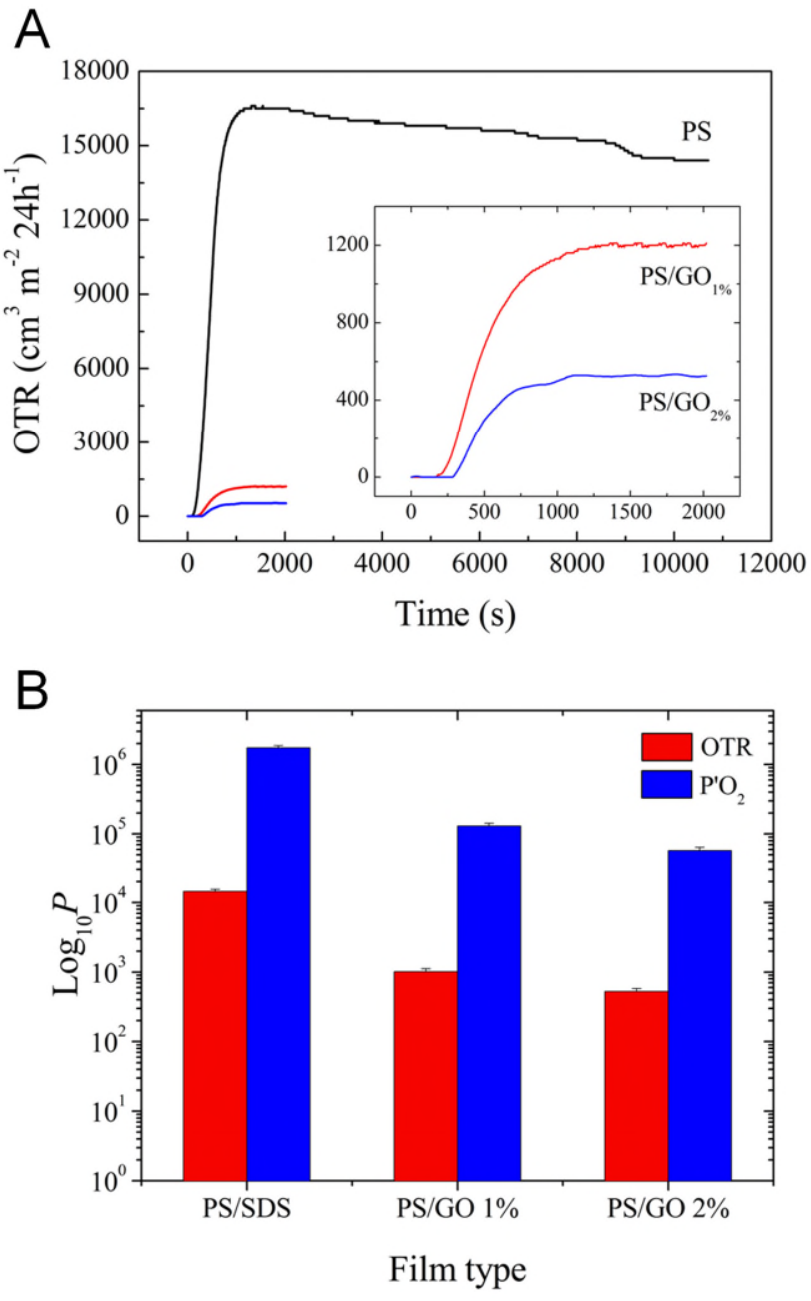

Figure 4. (A) Representative curves of the OTR evolution recorded for the PS films (PS/SDS and PS/GO). The different duration of the analysis indicates a different time necessary to achieve a steady state condition for each sample type. Tests were carried out at 23°C and 80% RH. The mean thickness of the tested films was 180 ± 15 μm. (B) Overall evolution of OTR and P′O2 for

the three different films (PS, PS/$GO_{1\%}$, and PS/$GO_{2\%}$). The permeability parameter (P) is expressed as $\log_{10}$ to allow a better display of the experimental data.

When the OTR results are converted to oxygen permeability coefficient (P′O2, cm^3 μm m^{-2} 24^{-1} atm^{-1}), which accounts for the unit thickness,[41] the overall trend does not change significantly (PS/SDS ~ 1.74×10^6 cm^3 μm m^{-2} 24^{-1} atm^{-1}; PS/$GO_{1\%}$ ~ 1.30×10^5 cm^3 μm m^{-2} 24^{-1} atm^{-1}; PS/$GO_{2\%}$ ~ 5.78×10^4 cm^3 μm m^{-2} 24^{-1} atm^{-1}, Figure 4B). The significant reduction in OTR values, in conjunction with the low temperature, aqueous and simple reaction procedure highlights the effectiveness of these materials as industrially viable gas barrier coatings.

To demonstrate the advantage of the GO encapsulation method over pristine GO, PS/GO films were prepared by using direct solution mixing and casting method, and the oxygen permeability coefficient was gathered from the OTR experiments as follows: PS/$GO_{1\%\ (mix)}$ ~ 1.90×10^5 cm^3 μm m^{-2} 24^{-1} atm^{-1}; PS/$GO_{2\%\ (mix)}$ ~ 7.73×10^4 cm^3 μm m^{-2} 24^{-1} atm^{-1}, which is clearly ~ 46% and ~ 34% higher than the films prepared with the GO encapsulated PS microparticles.

This work demonstrated that the GO encapsulated PS microparticles facilitate the GO nanoplatelets to be dispersed homogeneously in the polymer matrix, as shown in Figure 5ab and Figure 6. The GO nanoplatelets are further oriented parallel to the film surface with an interlayer distance of 50.9 ± 7.12 nm during the compression-moulding process, as shown from the cross-section of a PS/$GO_{1\%}$ film in Figure 5c. The distribution of the GO nanoplatelets across the film thickness acts as a physical obstacle to the permeation of the oxygen molecules, which accounts for the exceptional oxygen barrier performance.

Figure 5. Optical microscope images of (a) PS/$GO_{1\%}$ and (b) PS/$GO_{2\%}$ films at 20× magnification. A 100× magnification image is shown in the inset for each sample. (c) TEM image of compression moulded film of PS/$GO_{1\%}$.

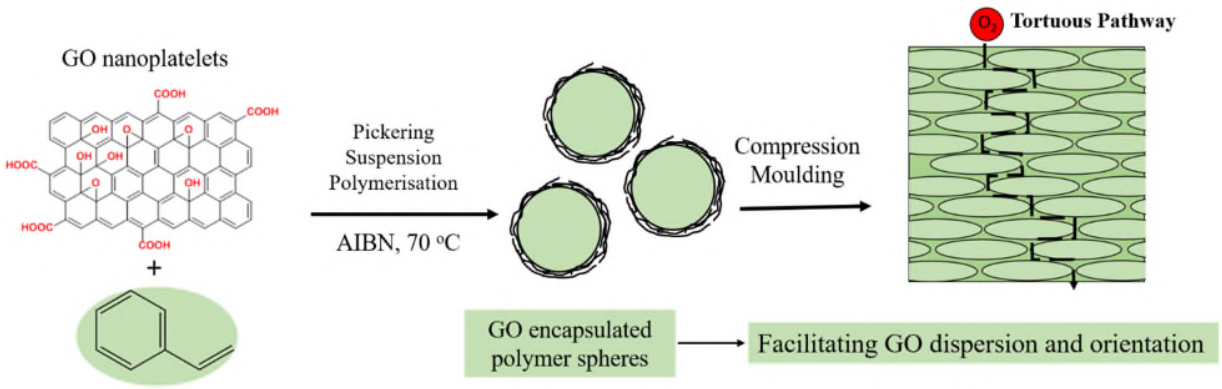

Figure 6 Schematic illustration showing the dispersion and orientation of GO nanoplatelets in polymers were facilitated by the GO encapsulated polymer method.

CONCLUSIONS

GO encapsulated PS microparticles were prepared by a facile Pickering suspension polymerization. The addition of NaCl had a charge screening effect that not only induced GO flocculation to the PS particle surface but also stimulated sedimentation of the encapsulated PS particles during polymerization. Compression moulding of the GO encapsulated PS microspheres at 190^{o}C did not cause detectable reduction of the GO sheets. A control PS film showed an OTR of 14464.67 cm^3 m^{-2} 24 h^{-1}, while the composite films of $PS/GO_{1\%}$ and $PS/GO_{2\%}$ displayed a reduction in OTR values by 93 and 96%, respectively. Due to the improved dispersion of GO by the polymer encapsulation process, alongside the nanoplatelets' orientation obtained by compression moulding, we have demonstrated the formation of highly effective gas barrier films.

The synthesis of GO encapsulated PS particles provided a viable process to produce high quality barrier films and coatings as well as a method that follows a green synthetic approach. The observed reduction in oxygen permeability is attributed to the tortuous pathway formed by stacking of the GO sheets and their well dispersed and oriented morphology within the polymer.

ASSOCIATED CONTENT

SUPPORTING INFORMATION

TGA analysis of PS/GO particles, optical microscope cross sections of PS/GO films, SEM imagery of PS/SDS particles and of 120^{o}C formed PS/GO film cross sections, Raman spectroscopy of PS/GO films formed at 120^{o}C and 190^{o}C and IR of PS/GO particles.

CORRESPONDING AUTHOR

Tel: +44 (0)24 7657 4038. Chaoying.wan@warwick.ac.uk

AUTHOR CONTRIBUTIONS

The manuscript was written through contributions of all authors. All authors have given approval to the final version of the manuscript.

ACKNOWLEDGMENT

We are grateful to the Polymer Characterisation RTP and Dr. Daniel Lester at University of Warwick for providing use of SEC equipment. SM thanks ESPRC and TATA steel for funding this PhD studentship. We are also grateful to the Advanced Bioimaging RTP and Dr. Saskia Bakker at University of Warwick for preparing samples for TEM.

REFERENCES

(1) Alexandre, M.; Dubois, P. Polymer-layered silicate nanocomposites: preparation, properties and uses of a new class of materials. *Materials Science and Engineering: R: Reports* **2000,** *28* (1), 1-63, DOI: https://doi.org/10.1016/S0927-796X(00)00012-7.
(2) Giannelis, E. P. Polymer layered silicate nanocomposites. *Advanced materials* **1996,** *8* (1), 29-35.
(3) Sideris, P. J.; Nielsen, U. G.; Gan, Z.; Grey, C. P. Mg/Al Ordering in Layered Double Hydroxides Revealed by Multinuclear NMR Spectroscopy. *Science* **2008,** *321* (5885), 113, DOI: 10.1126/science.1157581.
(4) Cui, Y.; Kundalwal, S.; Kumar, S. Gas barrier performance of graphene/polymer nanocomposites. *Carbon* **2016,** *98*, 313-333.
(5) Guan, Y.; Meyers, K. P.; Mendon, S. K.; Hao, G.; Douglas, J. R.; Trigwell, S.; Nazarenko, S. I.; Patton, D. L.; Rawlins, J. W. Ecofriendly Fabrication of Modified Graphene Oxide Latex Nanocomposites with High Oxygen Barrier Performance. *ACS Applied Materials & Interfaces* **2016,** *8* (48), 33210-33220, DOI: 10.1021/acsami.6b11554.
(6) Lu, C.; Mai, Y.-W. Influence of Aspect Ratio on Barrier Properties of Polymer-Clay Nanocomposites. *Physical Review Letters* **2005,** *95* (8), 088303, DOI: 10.1103/PhysRevLett.95.088303.
(7) Gorrasi, G.; Tortora, M.; Vittoria, V.; Pollet, E.; Lepoittevin, B.; Alexandre, M.; Dubois, P. Vapor barrier properties of polycaprolactone montmorillonite nanocomposites: effect of clay dispersion. *Polymer* **2003,** *44* (8), 2271-2279.
(8) Tasdelen, M. A.; Van Camp, W.; Goethals, E.; Dubois, P.; Du Prez, F.; Yagci, Y. Polytetrahydrofuran/Clay Nanocomposites by In Situ Polymerization and "Click" Chemistry Processes. *Macromolecules* **2008,** *41* (16), 6035-6040, DOI: 10.1021/ma801149x.
(9) Chang, K.-C.; Chen, S.-T.; Lin, H.-F.; Lin, C.-Y.; Huang, H.-H.; Yeh, J.-M.; Yu, Y.-H. Effect of clay on the corrosion protection efficiency of PMMA/Na+-MMT clay nanocomposite coatings evaluated by electrochemical measurements. *European Polymer Journal* **2008,** *44* (1), 13-23.

(10) Mballa, M. A. M.; Heuts, J. P.; van Herk, A. M. Encapsulation of non-chemically modified montmorillonite clay platelets via emulsion polymerization. *Colloid and Polymer Science* **2013,** *291* (3), 501-513.
(11) Mballa, M. A. M.; Heuts, J. P.; van Herk, A. M. The effect of clay on the morphology of multiphase latex particles. *Colloid and Polymer Science* **2013,** *291* (6), 1419-1427.
(12) Loiko, O. P.; Spoelstra, A. B.; van Herk, A. M.; Meuldijk, J.; Heuts, J. P. An ATRP-based approach towards water-borne anisotropic polymer–Gibbsite nanocomposites. *Polymer Chemistry* **2016,** *7* (20), 3383-3391.
(13) Loiko, O. P.; Spoelstra, A. B.; van Herk, A. M.; Meuldijk, J.; Heuts, J. P. Encapsulation of unmodified Gibbsite via conventional emulsion polymerisation using charged co-oligomers. *RSC Advances* **2016,** *6* (84), 80748-80755.
(14) Loiko, O. P.; Spoelstra, A. B.; van Herk, A. M.; Meuldijk, J.; Heuts, J. P. ATRP mediated encapsulation of Gibbsite: fixation of the morphology by using a cross-linker. *Polymer Chemistry* **2017,** *8* (19), 2909-2912.
(15) Loiko, O. P.; Spoelstra, A. B.; van Herk, A. M.; Meuldijk, J.; Heuts, J. P. Design and Preparation of Highly Filled Water-Borne Polymer–Gibbsite Nanocomposites. *Macromolecular Reaction Engineering* **2018,** *12* (1), 1700051.
(16) Mballa Mballa, M. A.; Ali, S. I.; Heuts, J. P.; van Herk, A. M. Control of the anisotropic morphology of latex nanocomposites containing single montmorillonite clay particles prepared by conventional and reversible addition-fragmentation chain transfer based emulsion polymerization. *Polymer International* **2012,** *61* (6), 861-865.
(17) Bhattacharya, M. Polymer Nanocomposites—A Comparison between Carbon Nanotubes, Graphene, and Clay as Nanofillers. *Materials* **2016,** *9* (4), 262.
(18) Tan, B.; Thomas, N. L. A review of the water barrier properties of polymer/clay and polymer/graphene nanocomposites. *Journal of Membrane Science* **2016,** *514*, 595-612.
(19) Yang, Y.-H.; Bolling, L.; Priolo, M. A.; Grunlan, J. C. Super Gas Barrier and Selectivity of Graphene Oxide-Polymer Multilayer Thin Films. *Advanced Materials* **2013,** *25* (4), 503-508, DOI: doi:10.1002/adma.201202951.
(20) Bon, S. A.; Colver, P. J. Pickering miniemulsion polymerization using laponite clay as a stabilizer. *Langmuir* **2007,** *23* (16), 8316-8322.
(21) Teixeira, R. F.; McKenzie, H. S.; Boyd, A. A.; Bon, S. A. Pickering emulsion polymerization using laponite clay as stabilizer to prepare armored “soft” polymer latexes. *Macromolecules* **2011,** *44* (18), 7415-7422.
(22) Chen, T.; Colver, P. J.; Bon, S. A. Organic–Inorganic Hybrid Hollow Spheres Prepared from TiO2-Stabilized Pickering Emulsion Polymerization. *Advanced Materials* **2007,** *19* (17), 2286-2289.
(23) He, Y.; Wu, F.; Sun, X.; Li, R.; Guo, Y.; Li, C.; Zhang, L.; Xing, F.; Wang, W.; Gao, J. Factors that Affect Pickering Emulsions Stabilized by Graphene Oxide. *ACS Applied Materials & Interfaces* **2013,** *5* (11), 4843-4855, DOI: 10.1021/am400582n.
(24) Liu, Y.; Zhang, Y.; Duan, L.; Zhang, W.; Su, M.; Sun, Z.; He, P. Polystyrene/graphene oxide nanocomposites synthesized via Pickering polymerization. *Progress in Organic Coatings* **2016,** *99*, 23-31.
(25) Xie, P.; Ge, X.; Fang, B.; Li, Z.; Liang, Y.; Yang, C. Pickering emulsion polymerization of graphene oxide-stabilized styrene. *Colloid and Polymer Science* **2013,** *291* (7), 1631-1639.

(26) Yin, G.; Zheng, Z.; Wang, H.; Du, Q.; Zhang, H. Preparation of graphene oxide coated polystyrene microspheres by Pickering emulsion polymerization. *Journal of colloid and interface science* **2013,** *394*, 192-198.
(27) Zhang, L.; Shi, T.; Wu, S.; Zhou, H. Graphene/polystyrene nanocomposites synthesized via pickering emulsion polymerization. *High Performance Polymers* **2014,** *26* (2), 156-165.
(28) Steward, P. A.; Hearn, J.; Wilkinson, M. C. An overview of polymer latex film formation and properties. *Advances in Colloid and Interface Science* **2000,** *86* (3), 195-267, DOI: https://doi.org/10.1016/S0001-8686(99)00037-8.
(29) Marathianos, A.; Liarou, E.; Anastasaki, A.; Whitfield, R.; Laurel, M.; Wemyss, A. M.; Haddleton, D. M. Photo-induced copper-RDRP in continuous flow without external deoxygenation. *Polymer Chemistry* **2019,** *10* (32), 4402-4406, DOI: 10.1039/C9PY00945K.
(30) Boyacı, D.; Iorio, G.; Sozbilen, G. S.; Alkan, D.; Trabattoni, S.; Pucillo, F.; Farris, S.; Yemenicioğlu, A. Development of flexible antimicrobial zein coatings with essential oils for the inhibition of critical pathogens on the surface of whole fruits: Test of coatings on inoculated melons. *Food Packaging and Shelf Life* **2019,** *20*, 100316, DOI: https://doi.org/10.1016/j.fpsl.2019.100316.
(31) Wei, P.; Luo, Q.; Edgehouse, K. J.; Hemmingsen, C. M.; Rodier, B. J.; Pentzer, E. B. 2D Particles at Fluid–Fluid Interfaces: Assembly and Templating of Hybrid Structures for Advanced Applications. *ACS applied materials & interfaces* **2018,** *10* (26), 21765-21781.
(32) Creighton, M. A.; Zhu, W.; van Krieken, F.; Petteruti, R. A.; Gao, H.; Hurt, R. H. Three-dimensional graphene-based microbarriers for controlling release and reactivity in colloidal liquid phases. *ACS nano* **2016,** *10* (2), 2268-2276.
(33) Quinn, M. D.; Vu, K.; Madden, S.; Notley, S. M. Photothermal Breaking of Emulsions Stabilized with Graphene. *ACS applied materials & interfaces* **2016,** *8* (16), 10609-10616.
(34) Farris, S. Engineering Properties of Packaging Films. In *Innovative Packaging of Fruits and Vegetables: Strategies for Safety and Quality Maintenance*; Apple Academic Press: 2018; pp 211-226.
(35) Yam, K. Gas permeation of packaging materials. *The Wiley Encyclopedia of Packaging Technology, third ed., John Wiley and Sons, Inc., New York* **2009**, 551-555.
(36) Cozzolino, C. A.; Campanella, G.; Türe, H.; Olsson, R. T.; Farris, S. Microfibrillated cellulose and borax as mechanical, O2-barrier, and surface-modulating agents of pullulan biocomposite coatings on BOPP. *Carbohydrate Polymers* **2016,** *143*, 179-187, DOI: https://doi.org/10.1016/j.carbpol.2016.01.068.
(37) Fukuzumi, H.; Saito, T.; Iwata, T.; Kumamoto, Y.; Isogai, A. Transparent and High Gas Barrier Films of Cellulose Nanofibers Prepared by TEMPO-Mediated Oxidation. *Biomacromolecules* **2009,** *10* (1), 162-165, DOI: 10.1021/bm801065u.
(38) Uysal Unalan. I.; Wan, C.; Figiel, L.; Olsson, R. T.; Trabattoni, S.; Farris, S. Exceptional oxygen barrier performance of pullulan nanocomposites with ultra-low loading of graphene oxide. *Nanotechnology* **2015,** *26*, 275703-275713. DOI: 10.1088/0957-4484/26/27/275703.
(39) Uysal Unalan, I.; Boyaci, D.; Ghaani, M.; Trabattoni, S.; Farris, S. Graphene oxide bionanocomposite coatings with high oxygen barrier properties. *Nanomaterials* **2016,** *6*, 244-254. DOI: 10.3390/nano6120244.
(40) Heo, J.; Choi, M.; Hong, J. Facile Surface Modification of Polyethylene Film Via Spray-Assisted Layer-By-Layer Self-Assembly of Graphene Oxide for Oxygen Barrier Properties. *Scientific Reports* **2019,** *9*, 2754. DOI:10.1038/s41598-019-39285-0.

(41) Fuentes-Alventosa, J. M.; Introzzi, L.; Santo, N.; Cerri, G.; Brundu, A.; Farris, S. Self-assembled nanostructured biohybrid coatings by an integrated ‘sol–gel/intercalation’approach. *RSC advances* **2013,** *3* (47), 25086-25096.